

Pitaya-Like Sulfur Electrodes by Chemically Anchored Polyaniline Shell for Lithium–Sulfur Batteries

Yan Wang^{1,*}, Wenxuan Wang²

¹ School of Information and Electronic Engineering, Hunan University of Science and Technology, Hunan 411201, China

² School of Materials Science and Engineering, Xiangtan University, Hunan 411105, China

*E-mail: ywang8@hnust.edu.cn

Received: 9 June 2016 / Accepted: 16 September 2017 / Published: 12 November 2017

Lithium–sulfur batteries are an attractive technology due to the light weight and low cost of sulfur, and a high theoretical specific capacity and specific energy compared to current lithium-ion batteries. However, a rapid capacity fade may occur which can be attributed mainly to polysulfide dissolution and volume expansion. To trap the polysulfides in the electrode of lithium–sulfur batteries and improve the electrochemical performances, we prepared a core–shell structure of polymer-coated sulfur cathode. By a simple two-step liquid phase reaction, a core-shell structural pitaya-like S/SiO₂@polyaniline (SSP) was first reported, which is expected to be catalytic for chemical reactions and able to adsorb lithium polysulphides. The results show that the SSP composites exhibited a high specific capacity and good cycling stability due to the role of complementary advantages of both polyaniline shell and SiO₂ particles for lithium–sulfur batteries. The SSP cathode delivered an initial specific discharge capacity of 850 mA h g⁻¹ and maintained 500 mA h g⁻¹ after 230 cycles at 0.5 C. The improvements of electrochemical performances may be attributed to the unique hybrid nanostructure of SSP and good dispersion of SiO₂ particles in sulfur.

Keywords: Polyaniline; Core–shell; Cathodes; Lithium–sulfur batteries

1. INTRODUCTION

Lithium–sulfur (Li–S) batteries have been one of the most promising candidates for high energy density applications especially in electric vehicles (EVs) and hybrid electric vehicles (HEVs), due to their high theoretical specific energy of 2600 W h kg⁻¹ and theoretical specific capacity of 1672 mA h g⁻¹ which is five times higher than that of the current lithium-ion batteries [1-4]. The high

capacity of such batteries is afforded by the reaction of $S_8 + 16Li^+ + 16e^- \longleftrightarrow 8Li_2S$ through long-chain lithium polysulfide intermediates Li_2S_x , $4 \leq x \leq 8$ [5-9].

However, the applications of the Li-S battery are limited by the large volume changes, poor electronic conductivity of sulfur, and the polysulfides dissolution in the electrolytes [10, 11]. To solve these problems, many attempts have been made to enhance the electrical conductivity of the cathode and suppress the polysulfide loss during cycling [12]. Various conductive carbon matrices [13-15], conducting polymers [16], and graphenes [17] have been used as host materials for the sulfur cathode in recent years to improve the electrochemical performance of Li-S batteries. A targeted approach is also adopted to bound polysulphides by the chemical interaction between the host and the lithium polysulphides [18]. For example, Yan and co-workers [19] have designed manganese dioxide nanosheet functionalized sulfur@poly(3,4-ethylenedioxythiophene) core-shell nanospheres for high performance Li-S batteries. Their study indicates that the functionalization of inorganic nanostructures on conducting polymer coated sulfur nanoparticles is an effective strategy to improve the electrochemical cycling performance and stability of sulfur cathodes for Li-S batteries. Zhou et al. [20] proposed the preparation of polydopamine-coated, nitrogen-doped, hollow carbon-sulfur in a double-layered core-shell architecture as an optimized design to confine the sulfur/polysulfides and keep intimate contact between sulfur and conductive carbon.

Recently, many oxide materials have been prepared to enhance the electrochemical performances of batteries by doping CuO [21, 22], TiO₂ [23], MnO₂ [1, 24], SiO₂ [25], Al₂O₃ [26] etc. Nevertheless, oxides have a lower conductivity than carbon materials, which would reduce the cycle stability and rate capability of lithium-sulfur battery. Therefore, there exist still a great challenge to effectively restrict the Li_2S_x into the electrolyte and improve the conductivity of active materials simultaneously. Until now, many efforts have been focusing on the preparation of novel nanostructures, such as core-shell structures [27, 28], primarily aiming to confining the active matter and mitigating the shuttling effect. Conducting polymers such as polypyrrole [1], polyaniline [27] and polythiophene [29] have been widely used for a conductive shell in lithium-sulfur battery cathode to improve the cycle performance and rate capability. Polyaniline is a specially promising conductive matrix for sulfur-contained composite for Li-S batteries due to its high absorption ability to sulfur and polysulfides [30]. For example, Zhou et al. [27] reported the synthesis of a polyaniline-sulfur yolk-shell nanocomposite through a heating vulcanization of a polyaniline-sulfur core-shell structure. They found that the heating treatment was more effective than chemical leaching to prepare yolk-shell structural electrodes. Sun et al. [31] synthesized a ternary polyaniline/sulfur/acetylene black composite cathode with variable polyaniline content by a continuous two-step liquid phase route.

In many cases SiO₂ is termed a "polysulfide reservoir," as in the work done by Ji et al. [32], wherein mesoporous silica was used as an additive in a mesoporous carbon/sulfur composite for a Li-S cathode structure. In that work it was demonstrated that the small amount of SiO₂ additive was necessary for trapping polysulfides and then readily desorbing them during electrochemical reduction/oxidation. In addition, the increased stability shown in the cycling of cathode composite was attributed to the mesoporous structure of the SiO₂, inhibiting diffusion of the polysulfide anions. Besides SiO₂, other oxides have been also shown to stabilize soluble polysulfide species, including Al₂O₃ [33] and La₂O₃ [34], often incorporated into nanocomposites with graphene or graphene oxide.

Due to the dual functions of SiO_2 as a structure building block and *in situ* polysulfide adsorbing agent, a good retention ability of polysulfides can be obtained for Li–S batteries [35]. Recently, Wei et al. [36] successfully synthesized ternary graphene/sulfur/ SiO_2 composite by compositing sulfur with graphene and then wrapping with SiO_2 . For the first time, Campbell et al. [37] fabricated the SiO_2 -coated sulfur particles *via* a facile two-step wet chemical process for application as a novel lithium–sulfur cathode material. Herein, inspired by the structure of pitaya, we presented a core-shell structural S/ SiO_2 @polyaniline composite used as cathode for lithium-sulfur battery. The SSP composite was made up of S/ SiO_2 core and polyaniline with a imitating the pitaya structure. The SSP composite is expected not only to relieve the shuttle effect of polysulfide and improve conductivity by polyaniline layer, but provide efficient polysulfide reservoirs by SiO_2 nanoparticles to trap the polysulfides and promote stable redox activity.

2. EXPERIMENTAL

2.1. Preparation of SSP composite

The synthesis process of the SSP composite is illustrated in Fig. 1. Firstly, a 500 mL of aqueous solution of $\text{Na}_2\text{S}_2\text{O}_3 \cdot 5\text{H}_2\text{O}$ (4.96 g) containing a small quantity of polyvinylpyrrolidone (PVP, $M_w \sim 55000$) (0.1 g) and silica with the size of 15 nm (0.1 g) was obtained. Then, 4 ml of concentrated hydrochloric acid was added dropwise to the solution when the mixture is mildly stirred. After chemical reaction for 2 h, the sulfur nanoparticles were collected by centrifugation for 10 minutes at 6 krpm and dispersed into a 0.05 wt% solution of PVP. The suspension was centrifuged for 10 minutes at 6 krpm twice using deionized water to prepare the pure S/ SiO_2 particles. The as-prepared S/ SiO_2 particles and PVP were dispersed in 150 ml of deionized water. Subsequently, a certain amount of aniline and concentrated hydrochloric acid (HCl) was added into the above emulsion under vigorous stirring. Then, ammonium persulphate ($(\text{NH}_4)_2\text{S}_2\text{O}_8$) dissolved in 50 ml of water was added dropwise to the above reactant mixture under magnetic stirring. After a stable stirring for 12 h at room temperature, the color of the suspension changed from white to greyish-green, indicating that SSP composites were synthesized. Then the composites were collected by centrifugation and dried under vacuum for one day.

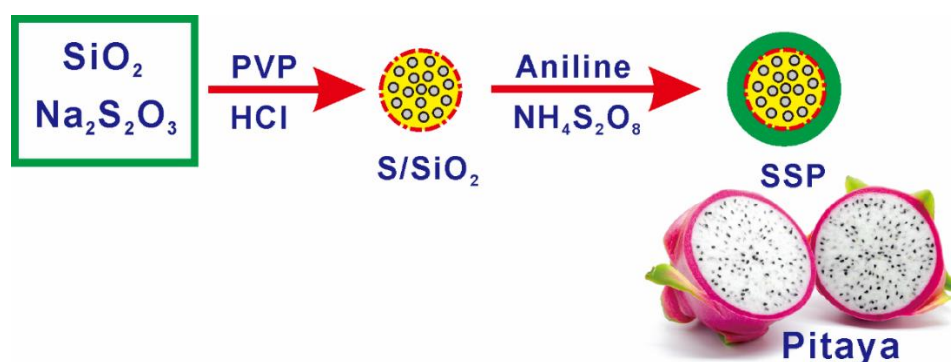


Figure 1. Schematic illustration of the synthesis process of SSP composite.

2.2. Materials Characterization

The powder X-ray diffraction (XRD, Rigaku D/max-2400) using Cu-K ($\lambda = 0.15406$ nm) radiation was employed to analyze the crystalline phase of SSP materials. Surface morphology was observed with scanning electron microscopy (SEM, JSM-5610LV) and microstructure was characterized through transmission electron microscopy (TEM, JEOL JEM-2100). The sulfur content was measured by thermogravimetric analysis (TGA, METTLER Toledo SMP/PF7548) under argon atmosphere with a temperature increase rate of $10\text{ }^{\circ}\text{C min}^{-1}$.

2.3. Electrochemical measurements

The positive electrode slurry was prepared by mixing SSP composite, acetylene black and PVDF (8:1:1 wt%) in N-methyl-2-pyrrolidone (NMP) solvent under continuous magnetic stirring for 5 h. The slurry was deposited on an aluminum foil substrate to form the cathodes and then the electrodes were dried at $60\text{ }^{\circ}\text{C}$ for 12 h in vacuum. The CR2016 coin cells were assembled in an Ar-filled glove box including a lithium metal anode, a Celgard 2400 separator and a cathode. The electrolyte was 1 M lithium bis (trifluoromethane) sulfonamide (LiTFSI) dissolved in a 1:1 volume ratio mixture of 1, 3-dioxolane (DOL) and dimethoxyethane (DME).

The galvanostatic charge/discharge tests were measured within the potential range of 1.7~3.0 V (vs. Li/Li⁺) at room temperature by using a BTS-5V3A battery test system. Cyclic voltammetry (CV) and electrochemical impedance spectroscopy (EIS) measurements were performed using a CHI660D electrochemical workstation (Chenhua, Shanghai, China). CV measurements were conducted between 1.5 V and 3.0 V (vs. Li/Li⁺) at a scanning rate of 0.05 mV s^{-1} .

3. RESULTS AND DISCUSSION

3.1. Microstructure characterization

The XRD patterns of sulfur, polyaniline and SSP composite are presented in Fig. 2. Polyaniline demonstrates an amorphous pattern with two wide peaks at $2\theta = 20^{\circ}$ and 25° , indicating periodic arrangement of polymer chains in parallel and perpendicular directions [38]. For the pure sulfur, the sharp and strong diffraction peaks match well with the typical S₈ structure, which agree well with the previous study [21]. The peaks of SSP composite centered at 23.4° and 28.0° match well with the sulfur (222) and (040) reflections of the *Fddd* orthorhombic phase of pure sulfur (JCPDS no. 08-0247). XRD of SSP composite shows it matches the combine of the pure sulfur and amorphous polyaniline.

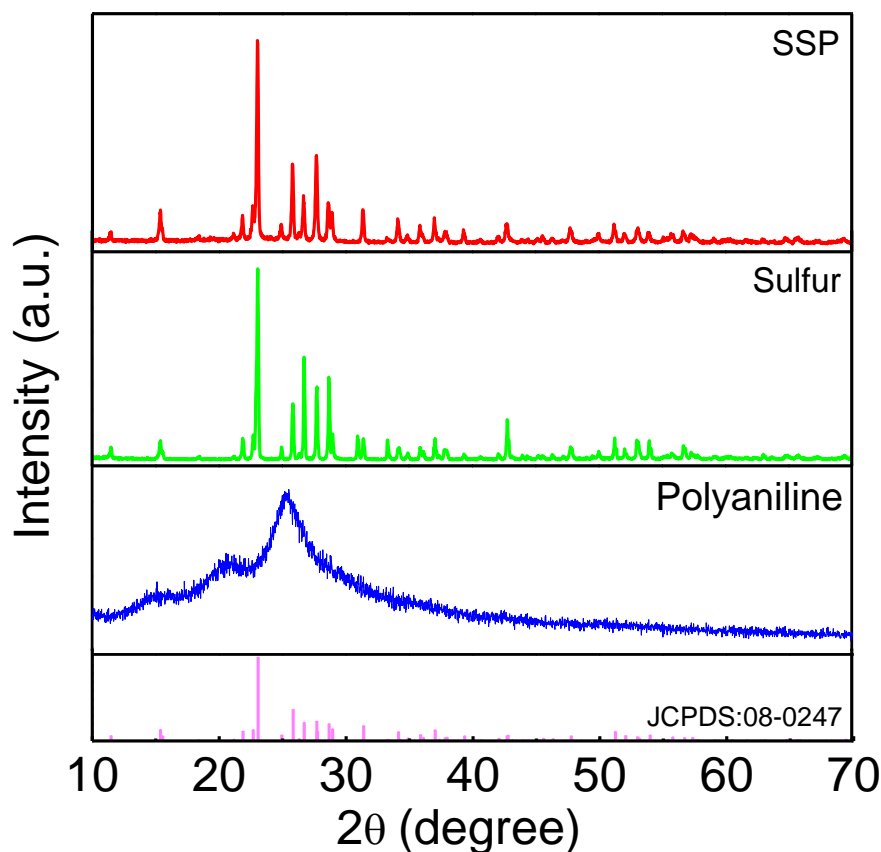


Figure 2. XRD patterns of SSP composite.

Fig. 3 shows the spherical SSP composite with an average diameter of 300 ± 30 nm. PVP molecules could form hollow microspheres in aqueous solution through a self-assembly process, with a special structure of the hydrophobic alkyl backbones toward the interior of hollow microspheres and the hydrophilic amide group outward into the water. Sulfur particles grows onto the hydrophobic portion of the PVP microspheres until the reaction is finished. EDS microanalysis exhibits a strong sulfur signal with the content of 26 wt% in SSP composite, as shown in Fig. 3c. Fig. 4 presents TEM images of SSP composite, and it is evident from the images that SSP composite exhibits a pitaya-like architecture consisting of a mixture of particles and core-shell. The SSP composite is spherical shape with a diameter of about 300 nm and the thickness of the polyaniline layer is about 25 nm. The inner S/SiO₂ particle is completely coated with polyaniline layer. To further confirm the core-shell structure of SSP composite, we removed the sulfur by using organic solvent, as shown in Fig. 4b. It is clear that the sulfur fills the interior of the polyaniline shell and the distribution of silica particles in the polyaniline layer is uniform. These results provided visible evidence that polyaniline has coated the S/SiO₂ particle, and the sulfur in the polyaniline coating could be recognized with SiO₂ particles.

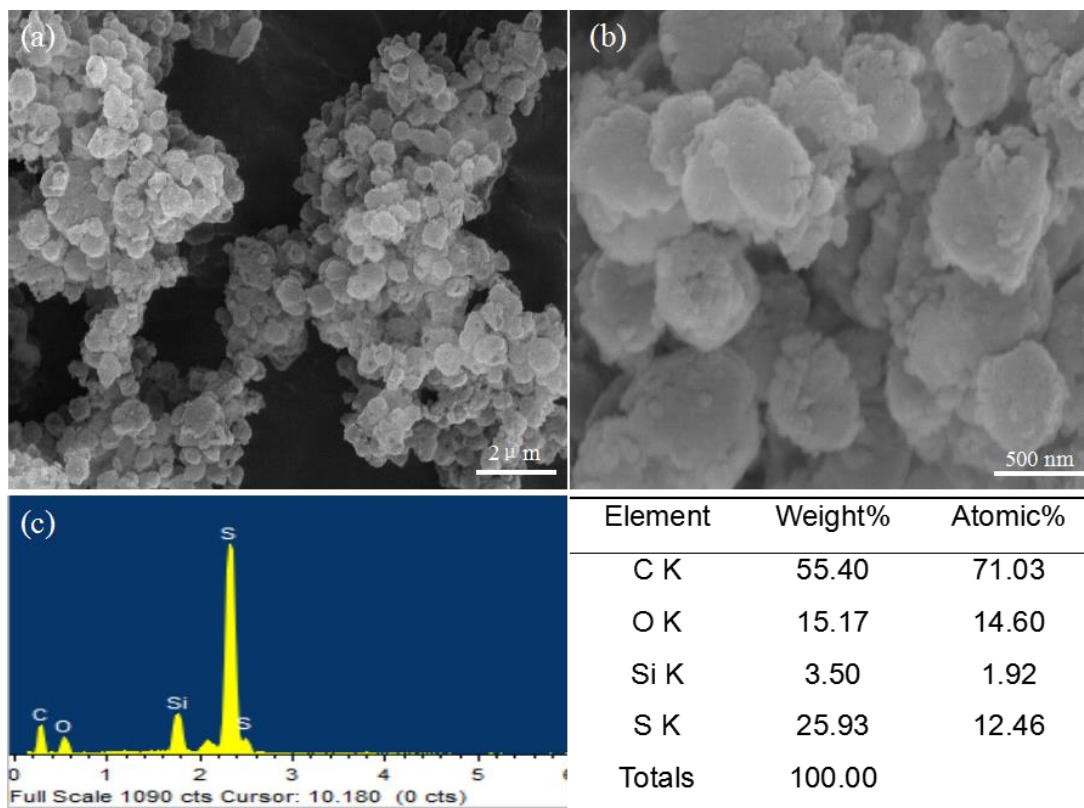


Figure 3. (a, b) SEM images and (c) EDS tests of SSP composite.

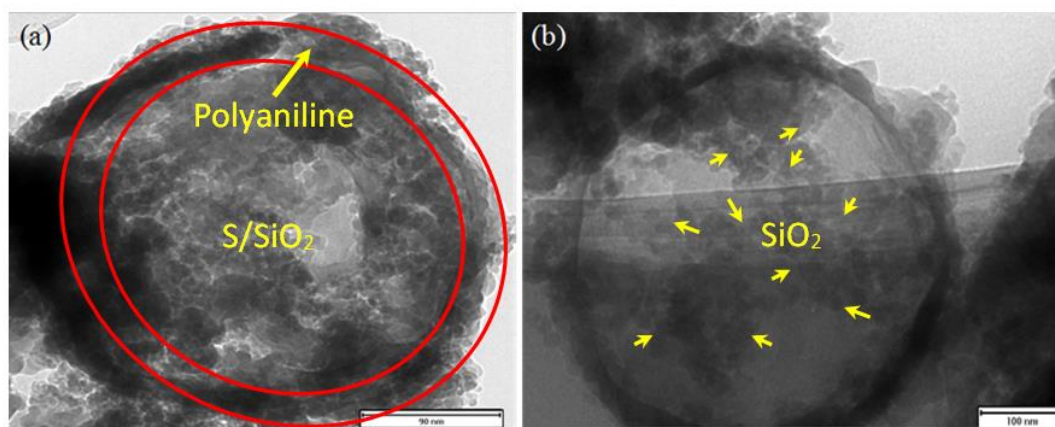


Figure 4. TEM images of SSP composite (a) before and (b) after removing sulfur.

Fig. 5 exhibits the thermogravimetric analysis of SSP composite and bare sulphur powder. The mass loss due to the sulphur evaporation occurs in the temperature range from 200 to 300 °C. The SSP composite has two main phase of weight-loss in the temperature range of 30 °C to 280 °C, in agreement with the literature data [39]. The first stage of mass loss is below 100 °C reflecting the evaporation of water in polyaniline and the second stage is at 200-280 °C corresponding to the loss of sulfur in composite materials. The sulfur content of the SSP composite is 60 wt% approximately.

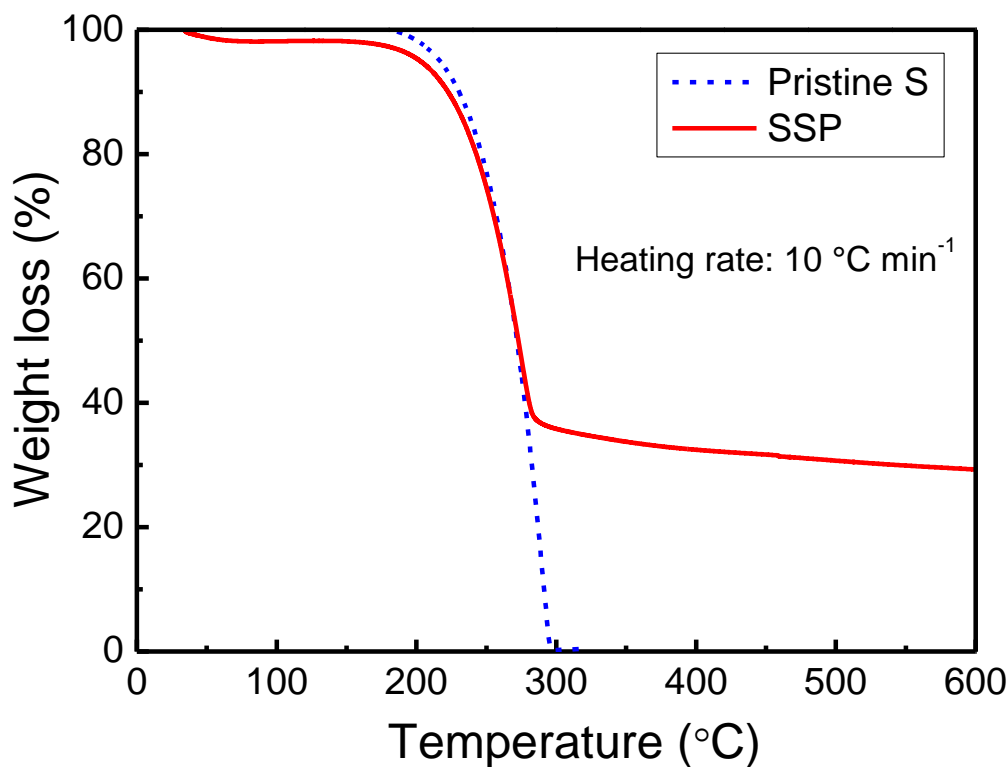


Figure 5. Thermogravimetric curves of sulfur and SSP composites.

3.2. Electrochemical performances

Fig. 6 shows the cyclic voltammograms of the SSP composite in the voltage window of 1.5–3.0 V, which are coincident with typical electrochemical reactions of elemental sulfur in the potential range 1.5–2.8 V. Two significant cathodic peaks are found at around 2.1 V and 2.3 V corresponding to two reduction processes, viz. the lithiation of S_8 to high order polysulfides (Li_2S_x , $4 \leq x \leq 8$) and further lithiation of Li_2S_4 to insoluble Li_2S_2/Li_2S , respectively. The anodic peak at 2.6 V represents the delithiation of Li_2S . It is also noted that, in the successive cycles, the two reduction peaks are relatively stable and the oxidation peak increases as the cycling increases because of the poor wettability between the active substance and electrolyte. The curves of 2nd and 3rd cycle are nearly overlapped, which indicates a good reversibility of the redox processes and high cycling stability of SSP cathode.

The initial discharge/charge curves of the lithium–sulfur batteries at 0.5 C ($1\text{ C} = 1672\text{ mA g}^{-1}$) and the cycling stabilities and Coulombic efficiencies of the SSP composite are shown in Fig. 7. It can be seen from Fig. 7a that there are two discharge potential plateaus and two charge potential plateaus in both discharge/charge profiles, which is consistent with the CV results. Furthermore, the voltage of discharge plateaus gradually deduces with increasing cycles due to the polarization caused by the dissolve of polysulfide into the electrolyte which can result in high viscosity of the electrolyte and slow migration rate of ion [40].

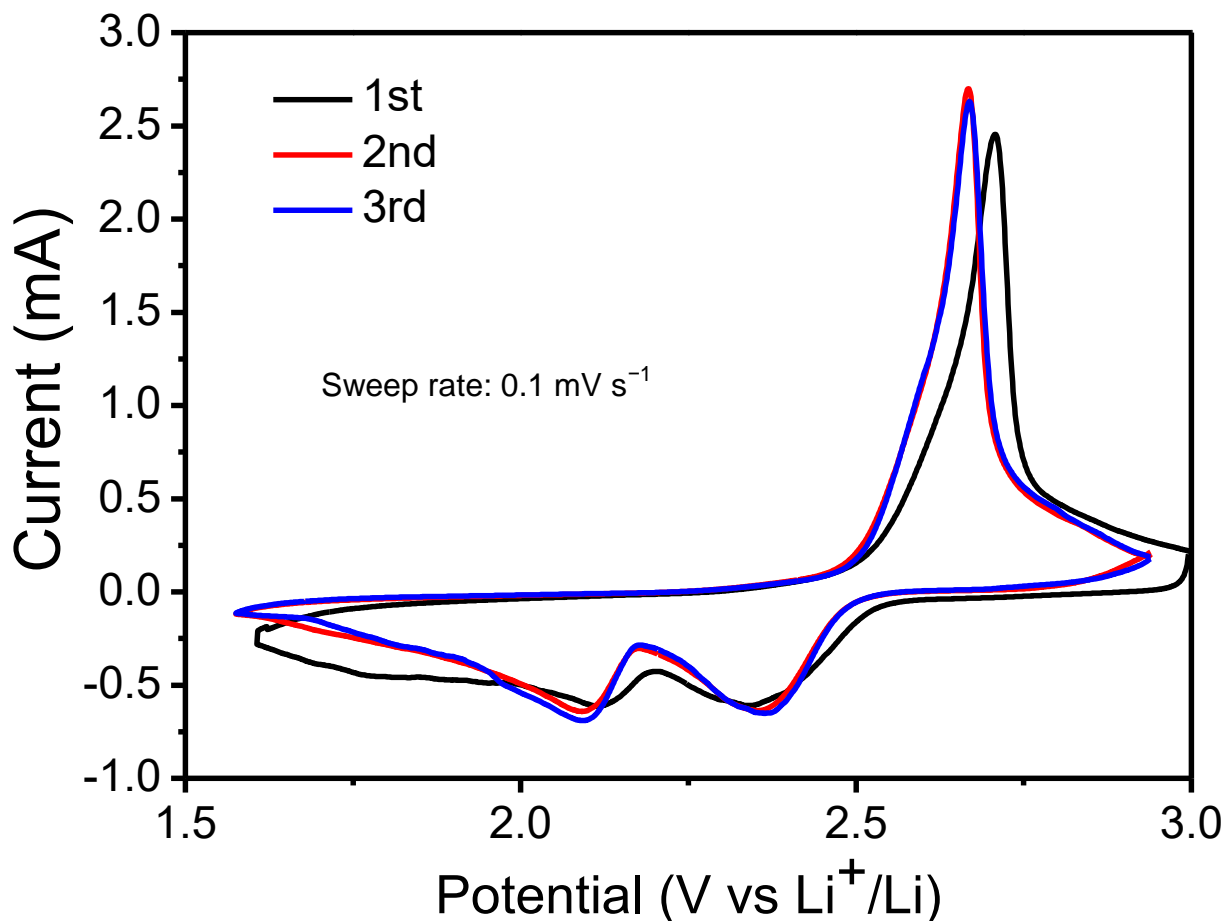


Figure 6. Typical CV curves of SSP composite.

Even though the structure may be gradually destroyed during the long cycle, the pitaya-like structure could suppress the diffusion of polysulfide into the electrolyte and improve the utilization of sulfur. A high initial specific capacity of up to 850 mA h g⁻¹ is obtained for SSP composite. Meanwhile, Fig. 7b shows the cycle performances of the SSP composite at a constant rate of 0.5 C. The discharge capacity of the SSP cathode retains 500 mA h g⁻¹ after 230 cycles with a capacity retention of 58.8%, demonstrating that the SSP electrode could effectively prevent the dissolution of polysulfide in the long-term cycle. It can be found that the coulombic efficiency of the SSP composite was beyond 95% at 0.5 C, further verifying that the shuttling effect of the polysulfides was relieved. Therefore, the superior performances may be attributed to the chemical adsorption of silica and the pitaya-like structure. Silica nanoparticles with larger specific surface could effectively trap polysulfides during electrochemical reduction/oxidation.

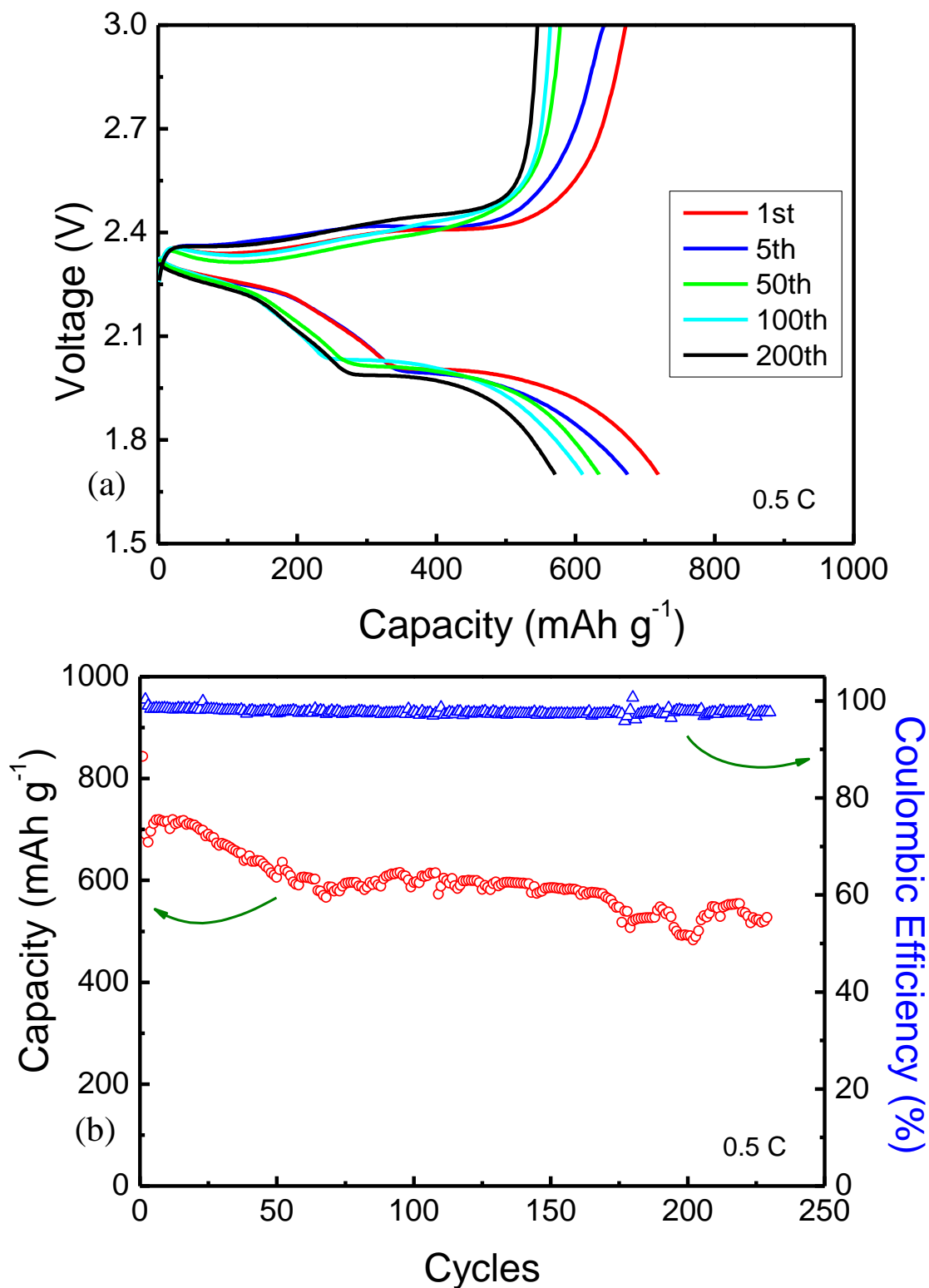


Figure 7. Electrochemical performances of SSP composite. (a) Charge–discharge voltage profiles and (b) Cycle performance and coulombic efficiency.

Rate capability of the cells with SSP composite cathode were also carried out at varied current rates from 0.2 to 2 C (1 C = 1672 mA g⁻¹), as shown in Fig. 8. The SSP cathode delivered a discharge capacity of 900 mA h g⁻¹ at 0.2 C, 730 mA h g⁻¹ at 0.5 C, 600 mA h g⁻¹ at 1 C rate, and 400 mA h g⁻¹

at 2 C rate, which is higher than the reported composites of sulfur and polyaniline, as shown in Table 1. However, for small current rates of 0.2 C and 0.5 C, yolk-shell sulfur-polyaniline composite exhibits a higher specific capacity than SSP in this study, which can be attributed to the internal void space to accommodate the volume expansion. After cycling at various rates, when the current rate was turned back to 0.2 C, a stable capacity of 800 mA h g⁻¹ is resumed after 50 cycles, which may benefit from the good conductivity of lithium ion by polyaniline and absorption effect of polysulfides by silica and polyaniline. The discharge (charge) plateaus gradually drop (rise) with the increasing rates, and the typical two plateaus in the discharge curves also declined in Fig. 8b. This is because of the polarization at high current densities and weak ion and electron conduction ability of the SiO₂ embedded in the sulfur hindering the fast dynamic reaction process of the SSP cathode.

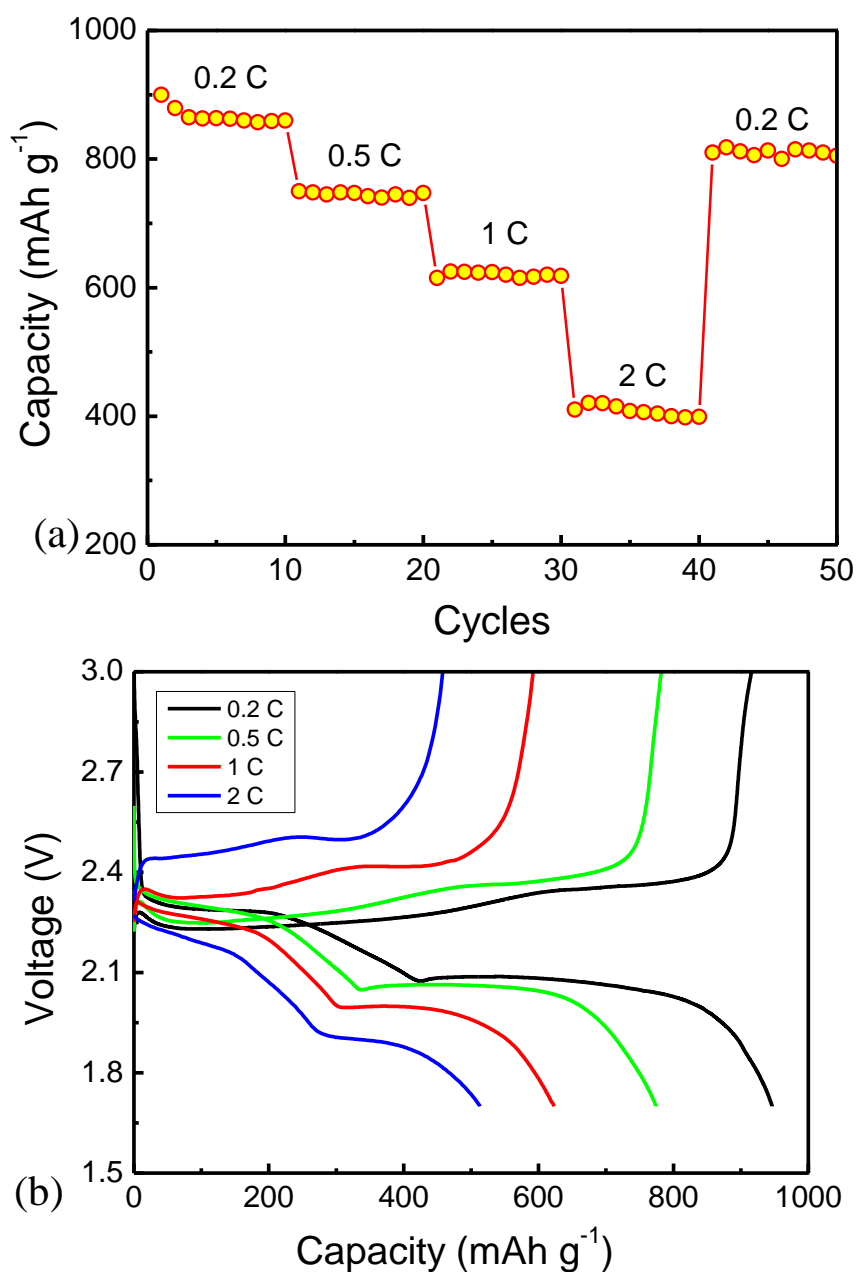


Figure 8. (a) Rate capability and (b) voltage profiles of SSP composite at various current densities.

Table 1. Comparison of specific capacities at different current rates for graphene/sulfur/polyaniline (GSP) [41], yolk-shell sulfur-polyaniline (SP) [27], carbon fibers/sulfur/polyaniline (CSP) [42], sulfur-polyaniline-graphene (SPG) [43] and SSP.

Current rate (C) (1 C = 1672 mA g ⁻¹)	Specific capacity (mA h g ⁻¹)				
	GSP	SP	CSP	SPG	SSP
0.2	550	1100	800	580	900
0.5	380	920	580	–	730
1	–	–	500	420	600
2	–	–	400	–	400

The superior cycle performance and rate capability of the SSP cathode is illustrated from the charge-transfer kinetics by the electrochemical impedance spectroscopy in Fig. 9. The semicircle in the high frequency region corresponds to the charge-transfer resistance of the electrolyte-electrode interface. The charge-transfer resistance values are 125 and 100 Ω for before and after 100 cycles, respectively, indicating an improved conductivity of the electrode and a better wetting of the electrolyte through the electrode due to the core-shell structure. Therefore, the EIS results further prove that the pitaya-like core-shell structure could suppress shuttle phenomenon in SSP cathode and improve the conductivity of the active substance and cycling stability.

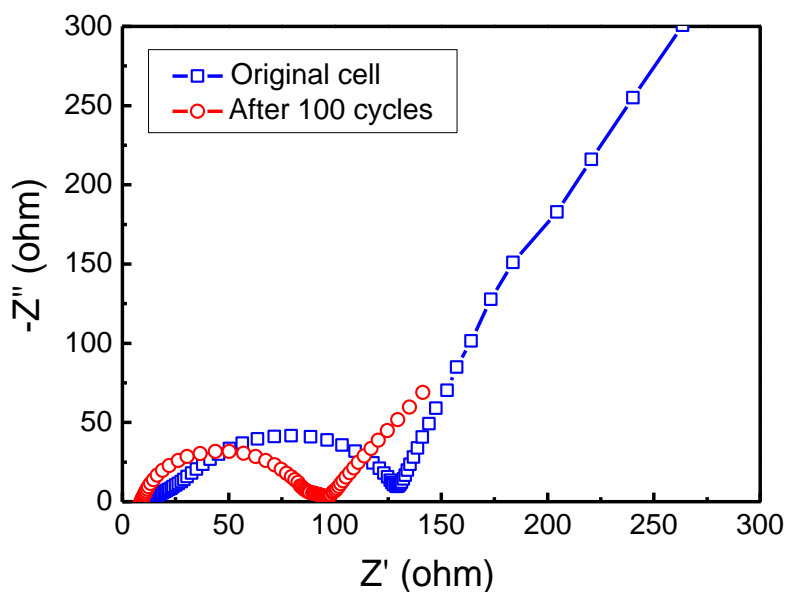


Figure 9. Nyquist plots of SSP cathode (a) before cycles and (b) after 100 cycles.

4. CONCLUSIONS

In summary, a pitaya-like core-shell structural S/SiO₂@polyaniline composite has been synthesized by the in-situ polymerization of aniline monomer on the silica nanoparticles and nano-sulfur spheres, which was inspired by the structure of pitaya architecture. Taking the advantage of

silica-doped sulfur particle and polyaniline-coated structure, the SSP cathode exhibited much improved cycling stability and columbic efficiency. The uniform and flexible polyaniline layer with a good electrical conductivity may play an important role in stability of the SSP composite during cycling. Meanwhile, the silica particles further are helpful to confine the sulfur particles inside the polyaniline shell, which facilitated to trap the polysulfides during the cycling processes and improve the cycling stability and efficiency. While slight capacity fading still remains in the SSP cathode, developing such a strategy is highly desirable because of the fact that these results provide promising insights and novel concepts for future Li–S batteries.

ACKNOWLEDGEMENT

This work has been supported by the National Natural Science Foundation of China (Grant Nos. 11372267 and 11402086).

References

1. X. Liang, C. Hart, Q. Pang, A. Garsuch, T. Weiss, L.F. Nazar, *Nat. Commun.*, 6 (2015) 5682.
2. C. Lai, Z. Wu, X. Gu, C. Wang, K. Xi, R.V. Kumar, S. Zhang, *ACS Appl. Mater. Interf.*, 7 (2015) 23885.
3. A. Fedorková, R. Oriňáková, O. Čech, M. Sedlaříková, *Int. J. Electrochem. Sci.*, 8 (2013) 10308.
4. W. Zhou, H. Chen, Y. Yu, D. Wang, Z. Cui, F.J. DiSalvo, H.D. Abruña, *ACS Nano*, 7 (2013) 8801.
5. P.G. Bruce, S.A. Freunberger, L.J. Hardwick, J.-M. Tarascon, *Nat. Mater.*, 11 (2012) 19.
6. Y.X. Yin, S. Xin, Y.G. Guo, L.J. Wan, *Angew. Chem. Int. Edit.*, 52 (2013) 13186.
7. Z. Li, Y. Pan, J. Cheng, J. Pan, L. Li, C. Wu, P. Gao, Z. Ma, *J. Polymer Mater.*, 32 (2015) 237.
8. J. Zhang, Z. Ma, J. Cheng, Y. Wang, C. Wu, Y. Pan, C. Lu, *J. Electroanal. Chem.*, 738 (2015) 184.
9. J. Cheng, Y. Pan, J. Zhu, Z. Li, J. Pan, Z. Ma, *J. Power Sources*, 257 (2014) 192.
10. J. Zhang, Z. Dong, X. Wang, X. Zhao, J. Tu, Q. Su, G. Du, *J. Power Sources*, 270 (2014) 1.
11. W. Zhou, C. Wang, Q. Zhang, H.D. Abruña, Y. He, J. Wang, S.X. Mao, X. Xiao, *Adv. Energy Mater.*, 5 (2015) 1401752.
12. S.-E. Cheon, K.-S. Ko, J.-H. Cho, S.-W. Kim, E.-Y. Chin, H.-T. Kim, *J. Electrochem. Soc.*, 150 (2003) A800.
13. Z. Zhang, Q. Li, Y. Lai, J. Li, *J. Phys. Chem. C*, 118 (2014) 13369.
14. X. Gu, Y. Wang, C. Lai, J. Qiu, S. Li, Y. Hou, W. Martens, N. Mahmood, S. Zhang, *Nano Res.*, 8 (2015) 129.
15. P. Pórolniczak, K. Wasiński, M. Walkowiak, *Int. J. Electrochem. Sci.*, 10 (2015) 9370.
16. S. Lim, R. Lilly Thankamony, T. Yim, H. Chu, Y.-J. Kim, J. Mun, T.-H. Kim, *ACS Appl. Mater. Interf.*, 7 (2015) 1401.
17. X. Yang, L. Zhang, F. Zhang, Y. Huang, Y. Chen, *ACS Nano*, 8 (2014) 5208.
18. Z. Li, J. Zhang, X.W.D. Lou, *Angew. Chem. Int. Edit.*, 54 (2015) 12886.
19. M. Yan, Y. Zhang, Y. Li, Y. Huo, Y. Yu, C. Wang, J. Jin, L. Chen, T. Hasan, B. Wang, B.-L. Su, *J. Mater. Chem. A*, 4 (2016) 9403.
20. W. Zhou, X. Xiao, M. Cai, L. Yang, *Nano Lett.*, 14 (2014) 5250.
21. C. Zu, A. Manthiram, *Adv. Energy Mater.*, 3 (2013) 1008.
22. K. Chen, Y. Dong Noh, K. Li, S. Komarneni, D. Xue, *J. Phys. Chem. C*, 117 (2013) 10770.
23. Z.W. Seh, W. Li, J.J. Cha, G. Zheng, Y. Yang, M.T. McDowell, P.-C. Hsu, Y. Cui, *Nat. Commun.*, 4 (2013) 1331.
24. K. Chen, D. Xue, *J. Mater. Chem. A*, 4 (2016) 7522.

25. S. Rehman, S. Guo, Y. Hou, *Adv. Mater.*, 28 (2016) 3166.
26. Z. Zhang, Y. Lai, Z. Zhang, K. Zhang, J. Li, *Electrochim. Acta*, 129 (2014) 55.
27. W. Zhou, Y. Yu, H. Chen, F.J. DiSalvo, H.c.D. Abruña, *J. Am. Chem. Soc.*, 135 (2013) 16736.
28. J. Liu, H. Xia, D. Xue, L. Lu, *J. Am. Chem. Soc.*, 131 (2009) 12086.
29. F. Wu, J. Chen, R. Chen, S. Wu, L. Li, S. Chen, T. Zhao, *J. Phys. Chem. C*, 115 (2011) 6057.
30. L. Xiao, Y. Cao, J. Xiao, B. Schwenzer, M.H. Engelhard, L.V. Saraf, Z. Nie, G.J. Exarhos, J. Liu, *J. Mater. Chem. A*, 1 (2013) 9517.
31. Y. Sun, S. Wang, H. Cheng, Y. Dai, J. Yu, J. Wu, *Electrochim. Acta*, 158 (2015) 143.
32. X. Ji, S. Evers, R. Black, L.F. Nazar, *Nature Commun.*, 2 (2011) 325.
33. M. Yu, W. Yuan, C. Li, J.-D. Hong, G. Shi, *J. Mater. Chem. A*, 2 (2014) 7360.
34. F. Sun, J. Wang, D. Long, W. Qiao, L. Ling, C. Lv, R. Cai, *J. Mater. Chem. A*, 1 (2013) 13283.
35. K.H. Kim, Y.-S. Jun, J.A. Gerbec, K.A. See, G.D. Stucky, H.-T. Jung, *Carbon*, 69 (2014) 543.
36. P. Wei, M. Fan, H. Chen, D. Chen, C. Li, K. Shu, C. Lv, *Int. J. Hydrogen Energy*, 41 (2016) 1819.
37. B. Campbell, J. Bell, H.H. Bay, Z. Favors, R. Ionescu, C.S. Ozkan, M. Ozkan, *Nanoscale*, 7 (2015) 7051.
38. F. Xu, G. Zheng, D. Wu, Y. Liang, Z. Li, R. Fu, *Phys. Chem. Chem. Phys.*, 12 (2010) 3270.
39. J. Wang, J. Chen, K. Konstantinov, L. Zhao, S.H. Ng, G. Wang, Z. Guo, H. Liu, *Electrochim. Acta*, 51 (2006) 4634.
40. G.C. Li, G.R. Li, S.H. Ye, X.P. Gao, *Adv. Energy Mater.*, 2 (2012) 1238.
41. P. Wei, M. Fan, H. Chen, X. Yang, H. Wu, J. Chen, T. Li, L. Zeng, Y. Zou, *Electrochim. Acta*, 174 (2015) 963.
42. L. Zhou, H. Mao, A. Yu, *J. Electroanal. Chem.*, 761 (2016) 62.
43. L. Li, G. Ruan, Z. Peng, Y. Yang, H. Fei, A.-R.O. Raji, E.L.G. Samuel, J.M. Tour, *ACS Appl. Mater. Interf.*, 6 (2014) 15033

© 2017 The Authors. Published by ESG (www.electrochemsci.org). This article is an open access article distributed under the terms and conditions of the Creative Commons Attribution license (<http://creativecommons.org/licenses/by/4.0/>).